Supporting Information for:

Nanoenabled direct contact interfacing of syringe-injectable mesh electronics

Jung Min Lee,[†,‡,§] Guosong Hong,[†,∥,§] Dingchang Lin,[†,§] Thomas G. Schuhmann, Jr.,[#] Andrew T. Sullivan,[#] Robert D. Viveros,[#] Hong-Gyu Park,[,‡] and Charles M. Lieber*[,†,#,⊥]*

[†]Department of Chemistry and Chemical Biology, Harvard University, Cambridge, MA, USA. [‡]Department of Physics, Korea University, Seoul, Republic of Korea. [∥]Department of Materials Science and Engineering, Stanford University, Stanford, CA, USA. [#]John A. Paulson School of Engineering and Applied Sciences, Harvard University, Cambridge, MA, USA. [⊥]Center for Brain Science, Harvard University, Cambridge, MA, USA.

Corresponding Authors.

*E-mail: hgpark@korea.ac.kr

*E-mail: cml@cmliris.harvard.edu

This file includes:

Materials and Methods

Double-sided input/output (I/O) pads design parameters

The syringe-injectable mesh probes with exposed gold (Au) metal on both sides of the I/O pads, termed "double-sided I/O pads", have three key parts: (1) implanted mesh with Pt electrodes for neural recording; (2) stem containing Au metal interconnect lines connecting the recording electrodes to the I/O part; and (3) I/O pads that connect individual channels to an external recording instrumentation interface (Figure S1; Figure S2).

The mesh part was fabricated using a similar process as described in previous reports,[1-4] with key dimensions (Figure S1b) as follows: (i) longitudinal SU-8 element width, W_1 = 10 μm and transverse SU-8 element width, W_2 = 10 μm; (ii) angle between longitudinal and transverse SU-8 element, α_1 = 45°; (iii) longitudinal element pitch, L_1 = 330 μm, and transverse element pitch, L_2 = 125 μm; (iv) metal interconnect line width, W_m = 1.5 μm with two interconnect lines in each longitudinal element, such that each interconnect line is 2.5 μm from the element edge, and 2 μm from the adjacent interconnect line in the same element; (v) a total of 17 longitudinal elements; (vi) Pt electrode diameter, 20 μm; (vi) longitudinal span of Pt electrodes, 2 mm; (viii) thickness of the three-layer structure (SU-8/metal/SU-8) in longitudinal elements, 400 nm/100 nm/400 nm; and (ix) thickness of the two-layer structure (SU-8/SU-8) in transverse elements, 400 nm/400 nm.

The stem part is composed of a single contiguous insulating layer encapsulating all of the metal interconnects. The key dimensions of the stem part (Figure S1c) are as follows: (i) total SU-8 width, W_s = 150 μm; (ii) metal interconnect line width, W_m = 1.5 μm; and (iii) thickness of the three-layer structure (SU-8/metal/SU-8), 400 nm/100 nm/400 nm.

We specify the dimensions of the individual I/O pads using the following key design parameters (Figure S1d): (i) a unit cell of I/O pad dimensions 50 μm × 50 μm; (ii) cross-sectional Au/SU-8/Au thickness of T = 100 nm/T_1 = 100 nm/T = 100 nm; (iii) total I/O pad width, a = 200 μm and gap between I/O pads, b = 300 μm; (iv) I/O pad length, l = 100 μm; (v) longitudinal and transverse Au ribbon width, W_3 = 10 μm; and (vi) longitudinal and transverse thin SU-8 ribbon width, W_4 = 6 μm. These parameters result from two analyses performed to identify optimal I/O pad design in terms of mechanical and electrical properties, bending stiffness and contact resistance, and geometric properties which minimize the probability of electrical shorting.

First, in order to identify the geometry of I/O pad which produces optimal contact resistivity, thereby facilitating direct contact interfacing, we investigated the mechanical properties of continuous I/O meshes with four different unit cells (Figure S5a, design I-IV) and different thickness (Figure S5b ii, design IV*) with finite element analysis and experimentally determined contact resistivities of each design (Figure 2b, c, and d, and Figure S5). These designs are defined by the dimensions of their unit cells in the transverse (x) and longitudinal (y) directions, respectively as follows: design I, $\boldsymbol{x_1}$ = 100 μm, $\boldsymbol{y_1}$ = 100 μm; design II, $\boldsymbol{x_1}$ = 100 μm, $\boldsymbol{y_2}$ = 50 μm; design III, $\boldsymbol{x_2}$ = 50 μm, $\boldsymbol{y_2}$ = 50 μm; design IV and IV*, $\boldsymbol{x_3}$ = 25 μm, $\boldsymbol{y_3}$ = 25 μm (Figure S5a). All designs have an angle of 45° ($\boldsymbol{\alpha_2}$) between longitudinal and transverse Au ribbons, longitudinal and transverse Au ribbon widths of 10 μm, and longitudinal and transverse thin SU-8 ribbon widths of 6 μm. For designs I to IV, the cross-sectional Au/SU-8/Au layers have thicknesses of $\boldsymbol{T}$ = 100 nm/$\boldsymbol{T_1}$ = 100 nm/$\boldsymbol{T}$ = 100 nm (Figure S5b, i). For design IV*, the thickness of each layer is halved to $\boldsymbol{t}$ = 50 nm/$\boldsymbol{t_1}$ = 50 nm/$\boldsymbol{t}$ = 50 nm (Figure S5b, ii). While designs I, II, III and IV* all have reasonable bending stiffness and low contact resistivity below 2 × 10^{-2} Ω·cm^2, we selected design III for the mesh I/O pad unit cell in subsequent experiments as it exhibited the most facile handling and smoothest injection of mesh electronics. Thus, for all other results, including those presented in Figures 3 and 4 and Supplemental Figures S6 and S7, we design I/O pads with design III, $\boldsymbol{x_2}$ = 50 μm, $\boldsymbol{y_2}$ = 50 μm unit cells.

Second, the dimensions of individual I/O pads are explored using our method for rotational misalignment described below, as in Figure S3. Here, we consider the influence of geometric parameters $\boldsymbol{a}$ (the width of I/O pad), $\boldsymbol{b}$ (the gap between adjacent I/O pads), and $\boldsymbol{l}$ (the length of I/O pad) on the propensity for I/O pads to produce electrical shorting of adjacent flexible flat cable (FFC, 32 channels, 0.50 mm pitch, Au-coated leads, 2 in. length, Molex, part number 0150200339) leads as a function of rotational misalignment about the first I/O pad center. We designed an I/O pad width, $\boldsymbol{a}$, equal to the gap between adjacent FFC leads, $\boldsymbol{d}$, and the gap between I/O pads, $\boldsymbol{b}$, equal to the FFC lead width, $\boldsymbol{c}$, to prevent electrical shorts between I/O pads and FFC leads at 0°. To prevent shorting for angular misalignment up to 10°, the I/O pad length, $\boldsymbol{l}$, is set equal to one third of the FFC lead width, $\boldsymbol{c}$. Therefore, with $\boldsymbol{P_{FFC}}$ (the FFC lead pitch) of 500 μm and $\boldsymbol{c}$ (a lead width) of 300 μm, we obtain I/O pad geometry parameters, $\boldsymbol{a}$ = 200 μm, $\boldsymbol{b}$ = 300 μm, and $\boldsymbol{l}$ = 100 μm in Figure 1a, (iii).

Fabrication of mesh electronics with double-sided I/O pads

Key steps in the fabrication of mesh with double-sided I/O pads are as follows: (1) pre-cleaning of a 3"-diameter Si wafer (n-type 0.005 Ω·cm, 600-nm thermal oxide, Nova Electronic Materials) with oxygen plasma (100 W, 1 min, 50 sccm of O_2), followed by thermal evaporation (Thermal Evaporator, Sharon Vacuum) of a sacrificial Ni layer with a thickness of 100 nm; (2) cleaning with oxygen plasma (50 W, 1 min, 50 sccm of O_2), spin-coating with lift-off resist (LOR 3A, MicroChem Corp.) at 4000 rpm, baking at 185°C for 5 min, followed by spin-coating with positive photoresist (Shipley 1805, Microposit, The Dow Chemical Company) at 4000 rpm and baking for 2 min at 115°C; (3) photolithography (PL) patterning of the bottom Au I/O pads using a mask aligner (MA6 aligner, Karl Suss Microtec AG) at an energy density of 40 mJ/cm^2, development (MF-CD-26, Microposit, The Dow Chemical Company) for 50 s, thermal evaporation of 100 nm-thick Au layer, and then removal of Au-coated resist via liftoff (Remover PG, MicroChem Corp.). The deposition was performed at a high vacuum $< 1 \times 10^{-6}$ Torr; (4) spin-coating negative photoresist SU-8 (SU-8 2000.5, MicroChem Corp.) diluted in cyclopentanone (Sigma-Aldrich) to a ratio of 4:1 at 4000 rpm, followed by pre-baking at 65°C for 1 min and 95°C for 2 min, patterning by PL (energy density 100 mJ/cm^2), post-baking at 65°C for 1 min and 95°C for 2 min, development (SU-8 Developer, MicroChem Corp.) for 10 s, rinsing with isopropanol, and drying in a N_2 flow; (5) patterning of the bottom passivation layer by repeating step (4) using standard SU-8 2000.5, the same pre- and post-baking conditions and spinning speed, and development for 1 min followed by hard-baking for 90 min at 180°C; (6) patterning of the Au interconnect lines and the top I/O pad layer by repeating steps (2) and (3) with a 1.5 nm Cr layer and 100 nm-thick Au layer; (7) patterning of recording electrodes by repeating steps (2) and (3) with 1.5 nm Cr and 50 nm Pt layers deposited via electron-beam evaporation (E-beam Evaporator, Denton Vacuum) at a high vacuum $< 1 \times 10^{-6}$ Torr; (8) patterning of top SU-8 passivation layer by repeating step (5) to only expose the Au I/O pads and the Pt recording electrodes, followed by hard-baking again at 190-195°C for 90 minutes, which serves to promote diffusion of the two SU-8 layers at the interface to form a monolithic structure. Last, the Ni sacrificial layer is etched in a solution of 40% $FeCl_3$: 39% HCl: H_2O (1:1:20) to release the mesh electronics probes from the Si wafer. The released mesh electronics are rinsed in deionized (DI) water 5 times and transferred to a sterile 1× phosphate buffered saline (PBS) solution (HyClone™ Phosphate Buffered Saline, Thermo Fisher Scientific Inc.) for storage prior to injection.

Potential shorting of adjacent channels as a function of alignment angle

The choices of the geometric parameters $\boldsymbol{a}$, $\boldsymbol{b}$, and $\boldsymbol{l}$, (as in Figure S1d) are important for minimizing the potential shorting of adjacent leads on the FFC, while still permitting some degree of misalignment. We set an I/O pad width, $\boldsymbol{a}$, equal to the gap between adjacent FFC leads, $\boldsymbol{d}$, and the gap between adjacent I/O pads, $\boldsymbol{b}$, equal to a FFC lead width, $\boldsymbol{c}$ (Figure 1a, iii), as any other case would lead to a non-zero probability of shorting even in the case of perfect angular alignment ($\theta = 0^{o}$). To explore the role of these parameters in shorting when there is angular misalignment, we perform a simple geometric transformation using custom-written Matlab code to determine the location of each I/O pad in a linear n-channel array as a function of rotation about the center of the first I/O pad. In addition to the aforementioned I/O pad parameters, we must also specify the length of each metal FFC lead (in the vertical dimension), L_{FFC}, the width of the individual leads, $\boldsymbol{c}$, and the lead pitch, $\boldsymbol{P_{FFC}}$. This analysis allows us to estimate the smallest angle at which at least one of the I/O pads could short two adjacent metal leads in the FFC, assuming all I/O pads are aligned linearly with an angle θ to the horizontal axis. The horizontal coordinate of the center of the i^{th} FFC lead is determined as $\boldsymbol{C_{FFC,i}} = (i-1)*(\boldsymbol{a}+\boldsymbol{b})$, such that the first lead is centered at 0. The center coordinates for the i^{th} I/O pad are then $\boldsymbol{C_{x,i}} = \boldsymbol{C_{FFC,i}}\cos(\theta)$ and $\boldsymbol{C_{y,i}} = \boldsymbol{C_{FFC,i}}\sin(\theta)$. We then consider the rotation matrix, $\boldsymbol{R}$, for four points rotated about the origin, $R = \begin{bmatrix} \cos(\theta) & -\sin(\theta) \\ \sin(\theta) & \cos(\theta) \end{bmatrix}$, and define a 2 × 4 matrix for the four unrotated corners about (0,0), $Unrot = \begin{bmatrix} -\boldsymbol{l}/2 & -\boldsymbol{l}/2 & \boldsymbol{l}/2 & \boldsymbol{l}/2 \\ -\boldsymbol{a}/2 & \boldsymbol{a}/2 & -\boldsymbol{a}/2 & \boldsymbol{a}/2 \end{bmatrix}$. Then, the rotated corners are given by $Rot(:,i) = R * Unrot(:,i)$. Finally, we add the center coordinates for each of the n channels to obtain the location of the I/O pads shifted by the angle θ. We are ultimately interested in determining how variation of each of the relevant I/O pad parameters alters the propensity for shorting of adjacent channels as a function of rotational angle about the first I/O pad. In this context, shorting is identified by the presence of overlapping regions of a single I/O pad with both its adjacent FFC leads. After identifying these trends (Figure S3), we may determine optimal ranges for each parameter which balance the possibility of shorting with the ease of fabrication, handling, and alignment along the FFC.

Finite element analysis of I/O pad mechanical properties

The longitudinal (D_L) and transverse (D_T) bending stiffness of the five different I/O pad unit cells investigated in these studies, design I-IV and design IV*, were estimated using the

finite element software ABAQUS as previously described.[5,6] design I, x_1 = 100 μm, y_1 = 100 μm; design II, x_1 = 100 μm, y_2 = 50 μm; design III, x_2 = 50 μm, y_2 = 50 μm; design IV and IV*, x_3 = 25 μm, y_3 = 25 μm, with α_2 = 45° for all designs (Figure S5a). The cross-section for designs I-IV of the longitudinal and transverse elements was a 100 nm-thick SU-8 layer (T_1) sandwiched between two Au layers with thickness of 100 nm each (T), (Figure S5b, i). The cross-section for design IV* of the longitudinal and transverse elements was defined as a 50 nm-thick SU-8 layer (t_1) sandwiched between two Au layers with thickness of 50 nm each (t), (Figure S5b, ii). SU-8 and Au were modelled as linear elastic materials with Young's moduli of 2 GPa and 79 GPa, respectively. A small vertical displacement (v) was applied with the opposite end of the unit cell held fixed to estimate the associated external work (W_k), and the effective bending stiffness per width was estimated by

$$D = \frac{2\,W_k\,{T_U}^3}{3\,v^2\,L_U}$$

where T_U is the thickness of the unit cell perpendicular to the bending direction and L_U is the unit cell width parallel to the bending direction.[7]

In-vitro direct contact interface stability

To verify chronic direct contact interface stability, a single continuous mesh I/O pad consisting of the design III unit cell was mounted on FFC metal leads. To simulate conditions experienced by the interface during *in-vivo* trials without the need for surgical implantation, we prepared a mouse by fixing a head-stage on the skull. I/O pads were aligned on a FFC, which was glued to the head-stage and this interface was covered with epoxy and dental cement. Resistance measurements as function of distance were performed on days 1, 3, 7, 16, 24, and 33 to derive resistivity of I/O connection as a function of day after direct contact was made (Figure 2e).

Electrical Characterization

In-vitro impedance measurements of Pt electrodes in Figure 3c were carried out by immersing the electrodes in 1× PBS and using U1700 Series Handheld Capacitance/LCR Meter (U1731C, KEYSIGHT THECHNOLOGIES) at 1 kHz. Inter-channel impedance measurements between adjacent 1.5-μm-wide Au interconnects on three meshes (with an edge-to-edge distance of 2.5 μm) in Figure 3c were carried out with a ~5-mm portion of the SU-8 passivated Au

interconnects immersed in 1× PBS, which approximates the *in-vivo* recording environment, using an Agilent B1500A semiconductor device parameter analyzer (Agilent Technologies Inc.) with B1520AFG multifrequency capacitance measurement unit (Agilent Technologies Inc.) at a probing frequency of 1 kHz. *In-vivo* impedance measurements in Figure 4c were carried out using an Intan 512ch recording controller (Intan Technologies) at 1 kHz. We note that there are differences in recorded impedance values between the U1700 Series Handheld Capacitance/LCR Meter and Intan 512ch recording controller, although these differences are consistent across many measurements. This systematic difference is reflected in the slightly different values of impedance reported for *in-vitro* and *in-vivo* mesh measurements.

Vertebrate animal subjects

Adult (25-35 g) male C57BL/6J mice (Jackson Laboratory) were used as vertebrate animal subjects for multiplexed brain electrophysiology in this study. All procedures performed on the vertebrate animal subjects were approved by the Animal Care and Use Committee of Harvard University. The animal care and use programs at Harvard University meet the requirements of the Federal Law (89-544 and 91-579) and NIH regulations and are also accredited by the American Association for Accreditation of Laboratory Animal Care (AAALAC). Animals were group-housed on a 12 h: 12 h light: dark cycle in Harvard University's Biology Research Infrastructure (BRI) and fed with food and water ad libitum as appropriate.

Surgical implantation of fabricated double-sided I/O pad mesh electronics

Mice were anesthetized via intraperitoneal injection of a mixture of 75 mg/kg body weight ketamine (VetaKet, Patterson Veterinary Supply) and 1 mg/kg body weight dexdomitor (Dexdomitor, Orion Pharma) with the degree of anesthesia monitored using the toe pinch method. Body temperature was maintained at 37°C with a homeothermic blanket (Homeothermic Monitoring System, Harvard Apparatus). Mice were fixed in a stereotaxic frame (Lab Standard Stereotaxic Instrument, Stoelting Co.) after administration of anesthetic and ocular lubricant (Puralube Ophthalmic Ointment, Dechra Pharmaceuticals) was applied to prevent dryness during surgery. Mice were depilated using lotion (Nair, Church & Dwight) and the scalp was sterilized using surgical scrub (Betadine Surgical Scrub, Purdue Products). A 5 mm-long incision was made along the sagittal sinus and skin was resected so an area of *ca.* 5 mm × 5 mm was exposed using surgical scissors and a scalpel, which were sterilized by a bead sterilizer (Hot Bead Sterilizer, Fine Science Tools) for 1 h and 70% ethanol followed by rinsing

with DI water and sterile 1× PBS. A dental drill (Micromotor with On/Off Pedal 110/220, Grobet USA) was used to drill a 1 mm burr hole anterior to bregma into which a sterilized 0-80 set screw (18-8 stainless steel cup point set screw, outer diameter 1.52 mm, groove diameter 1.14 mm, length 4.76 mm; McMaster-Carr Supply Company) was inserted to serve as a point of fixation for the head stage. An identical hole was drilled on the opposite side of the midline and a sterile stainless-steel wire was inserted to a depth of *ca.* 500 μm to serve as the grounding and reference electrode.

3D-printed poly-lactic acid (PLA) head stages were sterilized with 70% ethanol. Stages were prepared by mounting two sterile FFCs folded into L shapes onto a piece of sterile poly-ethylene terephthalate (PET) fixed to the head stage with dental cement (Metabond Quick Adhesive Luting Cement, Parkell) as in Figure 4. FFCs on head stages were treated by oxygen plasma (50 W, 1 min, 50 sccm O_2) and DI water was dropped onto FFC leads to maintain surface hydrophilicity. Head stages were fixed to the skull and mounting screw with Metabond cement. 1 mm burr holes were drilled using a dental drill at the following stereotaxic coordinates to target the hippocampus in both hemispheres: AP -1.5 mm, ML ± 1 mm, and DV -2 mm. For implantation, a mesh electronics neural probe was loaded into a glass capillary needle with 300 μm inner and 400 μm outer diameters, which was inserted into a pipette holder with one end sealed by a circular screw fastener and epoxy. Capillary tubing was used to connect the pipette holder to a 1 mL syringe and the mesh was drawn into the needle from the PBS solution such that the double-sided I/O pad part, which is readily distinguished visually, was drawn in first, leaving the mesh electrode part near the tip of the needle. The loaded needle and pipette holder were mounted on the stereotaxic frame and connected to a syringe pump via the capillary tubing. PBS was applied to wet the mouse skull prior to needle insertion. After incising and resecting the dura with a sterile 27-gauge needle (PrecisionGlide, Becton Dickinson), the capillary needle was positioned above the burr hole and slowly lowered to the desired depth inside the brain according to the stereotaxic coordinates above. The mesh was injected using the field of view (FoV) method with a camera by balancing the upward motion of the needle and injection of the mesh.[8] Flow rates were typically between 5-20 mL/h and injected fluid volumes between 2.5-12.5 μL/mm length of injected mesh.

Mesh electronics neural probes were injected such that the mesh region with exposed Pt electrodes (Figure S1) was fully inside the brain while the I/O pads remained in the needle. The needle was moved to the position of the leads at the end of the FFC (previously fixed on the head stage) using the stereotaxic frame prior to ejecting the I/O pads from the needle onto

the FFC and aligning the row of mesh I/O pads with the FFC leads using a 1.1 mm inner diameter (ID) glass pipette (Disposable Pasteur Pipets, VWR International). If the I/O pads were misaligned with respect to FFC leads (i.e., alignment angle >10°; Figure S3), the I/O pads were pulled back into the capillary by applying negative pressure, and ejected onto the FFC metal leads until an alignment angle of <10° was achieved. Aligned I/O pads were fully dried with the aid of spear sponges (PVA Eye Spear, Ultracell) and fixed in place using quick drying adhesive (5 Minute Epoxy in DevTube, Devcon or UV Light Glue, Visbella), after which the interface was covered with Metabond cement. Antibiotic ointment was applied around the wound and the mouse was placed on a heating pad to recover. Mice were monitored during recovery and given 0.05 mg/kg body weight buprenorphine analgesic (Buprenex, Patterson Veterinary Supply) every 12 h for up to 72 h following surgery.

Recording and analysis of electrophysiological data

Mice were placed in a restrainer (Tailveiner Restrainer, Braintree Scientific) for recording. A custom-made printed circuit board (PCB) with a 32-channel zero-insertion force (ZIF) connector and a 32-channel Omnetics connector was used to provide parallel 32-channel connection from the head-mounted FFC to an Intan 32-channel amplifier (Intan RHD 2132, Intan Technologies) during recording measurements. Recordings were obtained using a sampling rate of 20 kHz and a 60 Hz notch filter. The electrophysiological recording data were analyzed offline. In brief, raw recording data were filtered using noncausal Butterworth band-pass filters ("filtfilt" function in Matlab) in the 250- to 6,000-Hz frequency range to extract single-unit spikes (Figure 4e, Figure S6, and Figure S7).[1] Single-unit spike sorting was performed by amplitude thresholding of the filtered traces with the threshold determined automatically based on the median of the background noise via the improved noise estimation method.[9] Detected spikes in each channel were clustered using the WaveClus software,[9] which performs unsupervised superparamagnetic clustering to identify recorded single neurons (Figure 4e, Figure S6, and Figure S7).

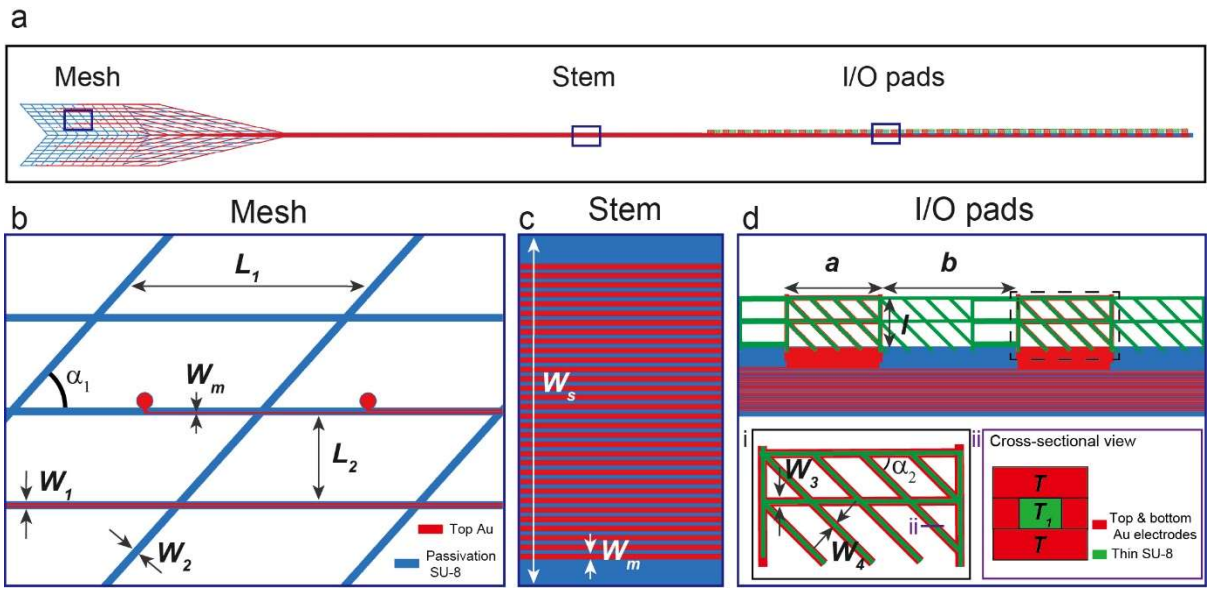

Figure S1. Overall design of mesh electronics neural probes. (a) Schematic of the mesh electronics probes composed of three regions: the implanted mesh; the stem; and the I/O pads. (b) Schematic of a portion of the implanted mesh with Pt-coated electrodes. Au metal interconnects run from the electrodes within the longitudinal SU-8 ribbons to individual I/O pads. Longitudinal and transverse SU-8 elements provide structural stability and electrical insulation. The macroporous structure allows the mesh to be precisely delivered using a needle and permits neuronal interpenetration for formation of a robust chronic electrode-tissue interface. Relevant design parameters of the mesh include: longitudinal element width, W_1 = 10 μm; transverse element width, W_2 = 10 μm; angle between transverse and longitudinal elements, α_1 = 45°; width of metal interconnect lines, W_m = 1.5 μm; pitch in longitudinal direction, L_1 = 330 μm; and pitch in transverse direction, L_2 = 125 μm. (c) Schematic of the stem connecting the mesh electrodes to the I/O pads. The stem contains all the metal interconnects encapsulated in a monolithic SU-8 structure for insulation. The metal interconnect line width is the same as in the mesh, W_m = 1.5 μm, and the total stem region width, W_s = 150 μm. (d) Schematic of two of the 32 I/O pads in 32-channel mesh probe. Each I/O pad carries the signal from a single mesh electrode to allow for multiplexed recording. Relevant design parameters include: width of I/O pads, a = 200 μm; gap between adjacent I/O pads, b = 300 μm; length of I/O pads, l = 100 μm; (i) width of Au elements in I/O pads, W_3 = 10 μm; width of supporting thin SU-8 elements, W_4 = 6 μm; angle between transverse and longitudinal elements in I/O pads, α_2 = 45°; (ii) cross-sectional thickness of bottom and top Au

layers with dashed line in (i), $\boldsymbol{T}$ = 100 nm each; and thickness of supporting thin SU-8 layer, $\boldsymbol{T_1}$ = 100 nm.

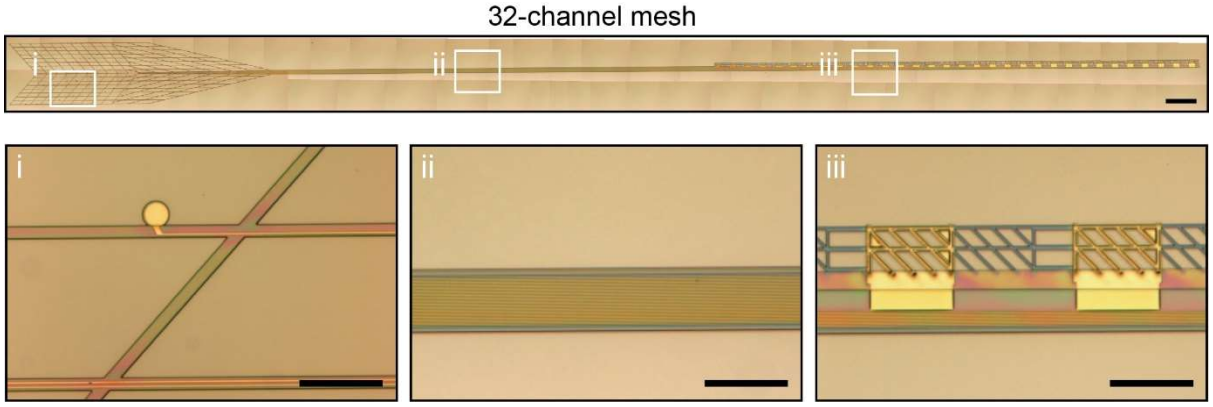

Figure S2. 32-channel mesh with double-sided I/O pads for direct contact. Optical microscope images of a 32-channel mesh probe. The full probe image (top) consists of 66 images stitched together to show the entire probe. The mesh part as in (i) was designed to contain two parallel channels in each longitudinal SU-8 ribbon, which terminate at Pt-coated recording electrodes at different longitudinal positions. All interconnects run through the stem part in (ii) and terminate at individual double-sided I/O pads in (iii), which provide parallel interfacing to an FFC via the direct contact electrical connection method. Scale bars are 1 mm for the top image and 200 μm for (i), (ii), and (iii), respectively. In addition, the same design principles can be used to further expand the total number of channels by including additional interconnects in the stem and corresponding I/O pads with dimensions appropriate to the metal leads of the interface. Thus, the direct-contact method with double-sided I/O pads, in principle, imposes no limitation on the number of parallel electrical connections.

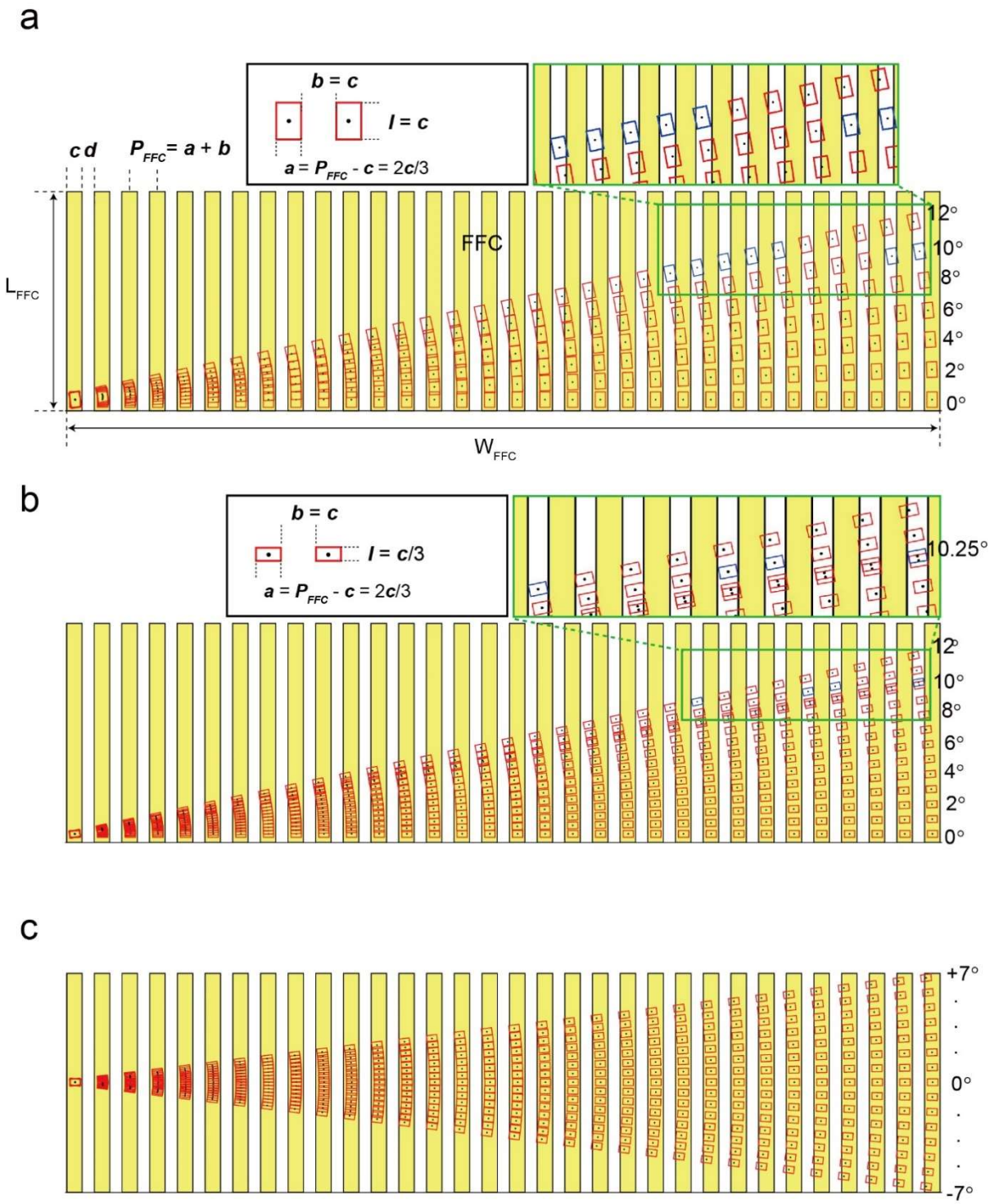

Figure S3. Design of I/O pad geometry to prevent shorting of adjacent channels. (a-c) Simulated results for location and extent of 32-channel I/O pads after alignment on the FFC leads, where 0° corresponds to perfect angular alignment and variation in angles represent cases of misalignment; the results were obtained using the information provided in the Materials and Methods. The row of I/O pads is rotated about the center of the leftmost I/O pad. Yellow stripes

represent leads on the FFC with length L_{FFC}, width c, gap d, and pitch P_{FFC} ($P_{FFC} = c + d$). The total FFC width is then $W_{FFC} = 31P_{FFC} + c$. Red open boxes represent I/O pads in the mesh electronics with width a, inter-pad gap b, and length l. Blue open boxes denote I/O pads that cause shorting between adjacent FFC leads. Here, we set an I/O pad width, a, equal to the gap between adjacent FFC leads, d, and the gap between I/O pads, b, equal to the FFC lead width, c, as any other case would lead to a non-zero probability of shorting even in the case of perfect angular alignment ($\theta = 0^o$). If the I/O pad width is larger than the gap between FFC leads ($a > d$), then lateral misalignment of the I/O pads to the center of the neighboring gap would cause shorting across all channels. To avoid this, we set $a = d$ to prevent shorting due to lateral misalignment alone for any case. For these calculations, the width-to-pitch ratio of the FFC leads is specified by our chosen FFC design, in which $c/P_{FFC} = 3/5$, so the upper bound on the I/O pad width is then $a = 2c/3$. (a) To investigate how the length (l) of the I/O pad affects angular misalignment, we begin by setting l equal to c. We consider increments of 2^o in the rotational misalignment angle, beginning at 0^o. The leftmost I/O pad is centered on the leftmost FFC lead horizontally, but closer to the bottom end of the FFC lead vertically. Results of these calculations reveal that, assuming perfect lateral alignment (i.e. the first I/O pad is centered on the first FFC lead along the horizontal dimension), shorting first occurs at the final I/O pad between 8^o and 10^o. At 10^o the final two I/O pads both exhibit overlapping regions along their adjacent leads, producing shorting of the final three FFC leads. Increasing the misalignment angle to 12^o further causes shorting between a group of 6 consecutive FFC leads produced by 5 adjacent I/O pads (top right magnified schematic). (b) Decreasing the I/O pad length to $l = c/3$ reduces the number of leads shorted to 0 at 10^o, and analysis using a finer grid of angles reveals that the first case of shorting does not occur until 10.25^o. Further increases in the rotational misalignment angle will cause shorting of channels shifted to the left part of the array, as in cases with longer pads. As a result of the reduction in the I/O pad length (l), even for angles from 10.25^o to 15^o, only one or two channels will be shorted. A maximum of two shorting pads is found for all cases up to 15^o, after which point the vertical length of the FFC leads becomes another limiting constraint in rotational misalignment. The limitation imposed by L_{FFC} becomes more pronounced for cases where the first I/O pad is farther from the bottom edge of the FFC lead. (c) The leftmost I/O pad is centered on the leftmost FFC lead both horizontally and vertically. This scenario limits the maximal angle of misalignment to $\pm 7^o$ due to the vertical length of the FFC leads and precludes any shorts between adjacent channels.

Thus, using the relationships $\boldsymbol{a} = \boldsymbol{P_{FFC}} - \boldsymbol{c} = 2\boldsymbol{c}/3$, and $\boldsymbol{l} = \boldsymbol{a}/2 = \boldsymbol{c}/3$, we are able to obtain a linear array of 32 I/O pads that is tolerant to rotational misalignment up to several degrees and only produces shorting of a few channels at larger misalignment angles. For the purposes of these calculations, we set $\boldsymbol{c}$ = 300 μm, $\boldsymbol{P_{FFC}}$ = 500 μm, $\boldsymbol{W_{FFC}}$ = 16 mm and $\boldsymbol{L_{FFC}}$ = 4 mm, to match the experimental parameters of the 32 channel FFC used in our studies but the method can be generalized to any arbitrary connector using similar analyses. Setting the width of the I/O pad equal to the gap between FFC leads and maintaining the aspect ratio ($\boldsymbol{l}/\boldsymbol{a}$ = 0.5) of the I/O pad produces qualitatively similar results for different FFC lead pitch and width. For width-to-pitch ratios of 0.2, 0.4, and 0.8, we can similarly observe the first cases of shorting occurring just after rotational misalignment angles of 10º, and further increases in misalignment angle produce small shorting regions of only a few pads. Hence, the FFC lead pitch, length, and width are all that is required to determine I/O pad geometry with maximal connection yield and minimal chance of shorts. The pitch controls the total width of the entire FFC and must necessarily be small enough to produce an acceptable spatial footprint. For a 500 μm pitch, the total width, $\boldsymbol{W_{FFC}}$, is only 16 mm. The FFC lead length, $\boldsymbol{L_{FFC}}$, is a limiting factor for the case of alignment along the center of the horizontal and vertical dimensions, and thus an increase in this parameter could produce a larger tolerance for misalignment. However, the tolerance would still then be limited by shorting, so this would only allow for an increase of up to ~3º. Finally, reducing the total number of electrodes, I/O pads, and FFC leads increases the rotational misalignment tolerance, given that the first half of the I/O pads are still not shorted at 10º, but this reduces the number of neurons that can be recorded simultaneously. It is also notable that using the reduced length of the I/O pads designed to reduce shorting of adjacent FFC leads also facilitates loading and injection of the I/O portion of the mesh through small diameter capillary needles used for implantation.

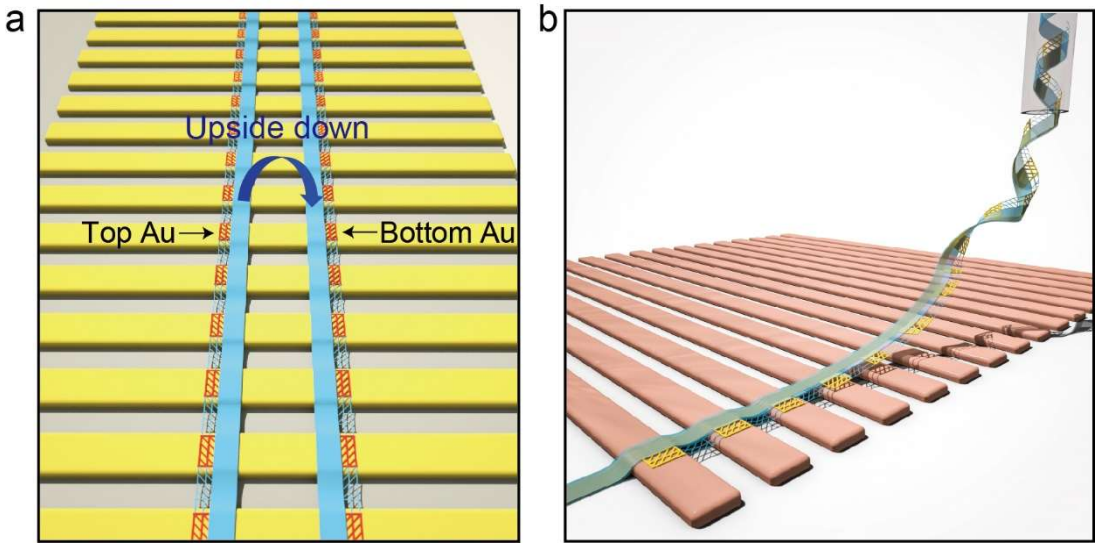

Figure S4. Double-sided I/O pad geometry for facile alignment on FFC. (a) Schematic of the I/O pads alignment to the FFC regardless of the side of the pad in contact with the leads. Each I/O pad is electrically continuous between the top and bottom Au layers, both of which are exposed to provide connection to the FFC. As a result, neuronal signals from the same channel can be transmitted and read out via the FFC leads regardless of whether the top or bottom face of the I/O pad is in contact with the FFC. (b) Schematic of the direct contact electrical connection method. The double-sided I/O pads ejected from the needle are positioned on the metal leads of the FFC to achieve multiplexed electrical contact after drying of ejected liquid. The configuration independence afforded by double-sided I/O pads greatly facilitates the formation of a robust electrical connection between all I/O pads and FFC leads, as the contacting side of the I/O pads cannot be controlled during ejection from the needle.

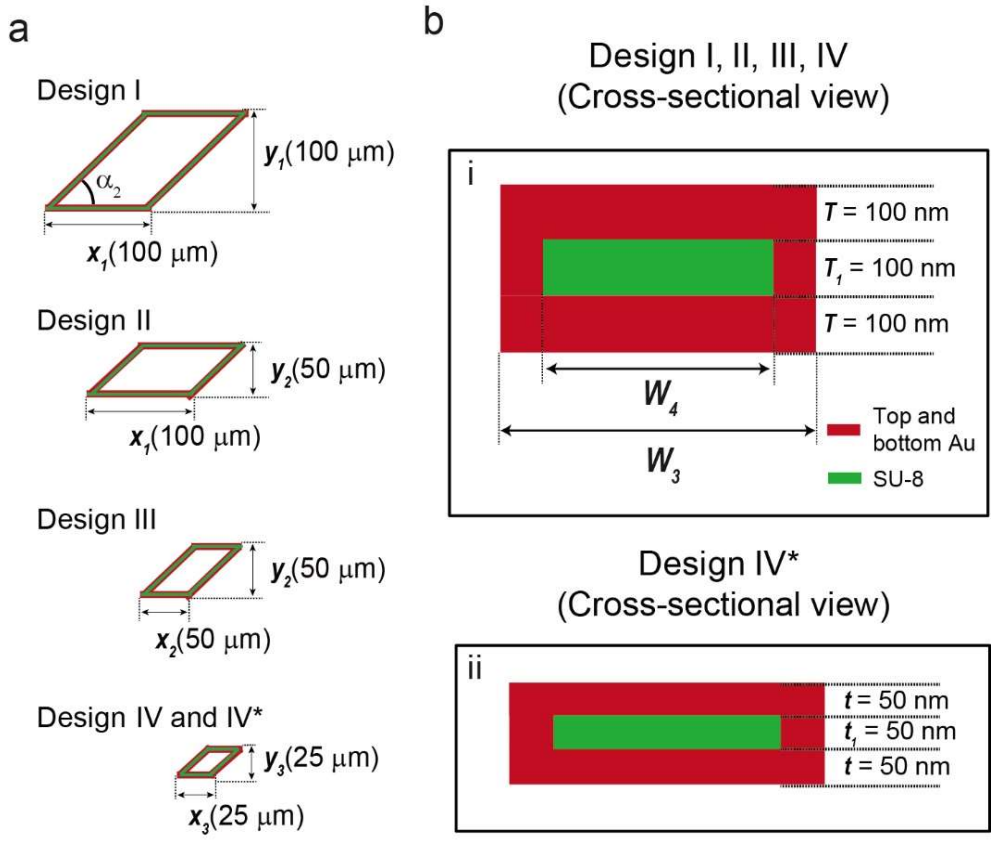

Figure S5. I/O pad unit cell designs for optimizing contact resistivity. (a) Schematics of four distinct unit cell geometries of the different I/O pad designs. These designs vary in size in the longitudinal and transverse directions as follows: design I, x_1 = 100 μm, y_1 = 100 μm; design II, x_1 = 100 μm, y_2 = 50 μm; design III, x_2 = 50 μm, y_2 = 50 μm; design IV and IV*, x_3 = 25 μm, y_3 = 25 μm. All designs have the same angle between the transverse and longitudinal elements in I/O pads, α_2 = 45°. (b) Cross-sectional schematics of designs I, II, III, IV and IV*. (i) Designs I, II, III, IV have the same cross-sectional profiles (Au 100 nm/SU-8 100 nm/Au 100 nm, $T/T_1/T$). (ii) For design IV*, the thicknesses of all three layers are halved (Au 50 nm/SU-8 50 nm/Au 50 nm, $t/t_1/t$).

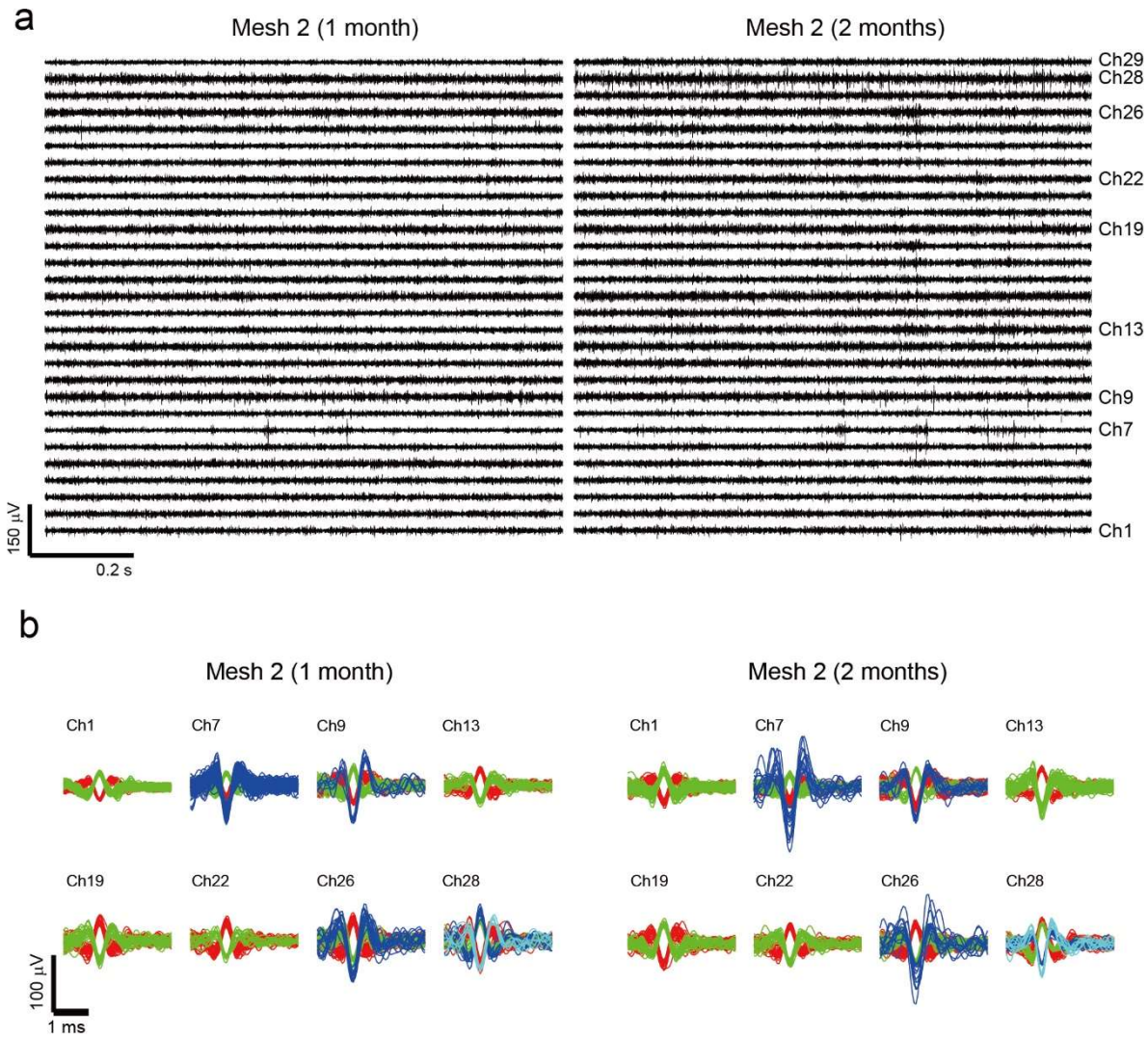

Figure S6. Chronically stable recordings of a second implanted mesh. (a) Electrophysiological recording data from the second mesh implanted in the mouse shown in Figure 4 at 1 and 2 months post-injection. The traces from 29 connected channels are shown after filtering with a noncausal Butterworth band-pass filter between 250 and 6,000 Hz. Electrical connection of 29 channels out of 32 was confirmed by measurement of electrical impedance at 1 kHz, which showed impedances of ~300 kΩ. (b) Spike sorting of recorded electrical traces in (a) for eight representative channels at both 1 month and 2 months post-injection. These eight channels recorded spikes from 21 single units at both time points, with comparable amplitude and waveform shape between the two time points. As in Mesh 1, no disconnection of channels was observed from 1 month to 2 months after mesh injection, highlighting chronic stability of the direct contact interface afforded by the mesh I/O pads.

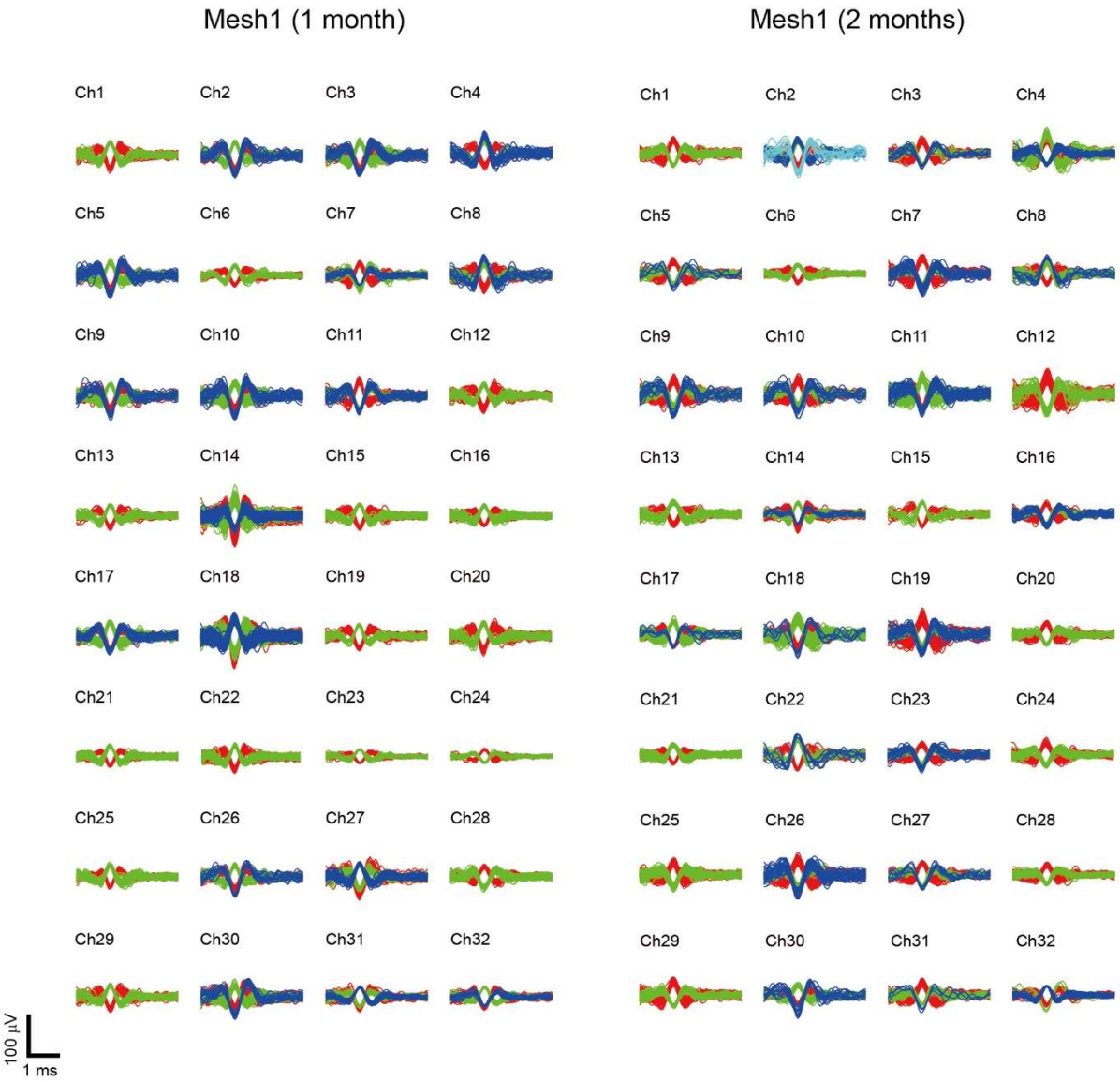

Figure S7. Spike sorting of recorded electrical traces to identify single units. Spikes were sorted from the electrical activity traces recorded from the 32 channels in Figure 4 using the WaveClus superparamagnetic clustering algorithm and automatic amplitude thresholding. Data from each channel were sorted at 1 month and 2 months post-injection. Most channels recorded activity from two or three neurons, with spikes recorded from 81 single units at 1-month post-injection and 86 single units at 2 months post-injection. No channels exhibited a decrease in the number of recorded single units during this time period. Waveform shape and amplitude appear stable between the two time points, consistent with the capability of mesh electronics to achieve chronically stable recording of individual neurons[1,2] and the chronic stability of the electrical interface between the I/O pads and FFC produced through the direct contact method.

Supplementary Video 1. *In vitro* I/O pad alignment on FFC. A 32-channel FFC was mounted on a glass slide using Metabond dental cement and treated with oxygen plasma for *in vitro* electrical connection yield quantification. The double-sided I/O pads from a 32-channel mesh electronics neural probe were aligned using the direct-contact method, as also shown in the sequential photographs in Figure 3a. The mesh part containing the recording electrodes was ejected onto the glass slide from a glass pipette filled with DI water while the I/O pads remained inside the pipette. The I/O pads were then unfolded along the leads of the FFC. If the misalignment angle was larger than 10º, the I/O pads were reloaded and realigned to ensure good electrical connection without shorting of adjacent channels. Play speed: 4× during injection and 2× during alignment.

Supplementary Video 2. *In vivo* I/O pad alignment on FFC following mesh injection. Two 32-channel mesh electronics probes were injected into the mouse hippocampus using the procedure described in Materials and Methods. After drilling holes for the grounding wire, mounting screw, and sites to target hippocampus (AP -1.5 mm, ML ±1 mm, and DV -2 mm), mesh electronics probes were sequentially injected and aligned using the field of view (FoV) method.[8] The mesh part of each probe was injected by balancing the flow rate with retraction of the needle, and the I/O pads were subsequently ejected onto the FFCs mounted on the head-stage. I/O pads were then aligned along the FFC leads with a final misalignment smaller than 10º. Play speed: 4× during injection and 2× during alignment.

Supplementary References

1. Fu, T.-M.; Hong, G.; Zhou, T.; Schuhmann, T. G.; Viveros, R. D.; Lieber, C. M. *Nat. Methods* **2016,** *13*, 875-882.
2. Fu, T.-M.; Hong, G.; Viveros, R. D.; Zhou, T.; Lieber, C. M. *Proc. Natl. Acad. Sci. U.S.A.* **2017,** *114*, E10046-E10055.
3. Schuhmann Jr, T. G.; Yao, J.; Hong, G.; Fu, T.-M.; Lieber, C. M. *Nano Lett.* **2017,** *17*, 5836-5842.
4. Hong, G.; Fu, T.-M.; Qiao, M.; Viveros, R. D.; Yang, X.; Zhou, T.; Lee, J. M.; Park, H.-G.; Sanes, J. R.; Lieber, C. M. *Science* **2018,** *360*, 1447-1451.
5. Liu, J.; Fu, T.-M.; Cheng, Z.; Hong, G.; Zhou, T.; Jin, L.; Duvvuri, M.; Jiang, Z.; Kruskal, P.; Xie, C.; Suo, Z.; Fang, Y.; Lieber, C. M. *Nat. Nanotechnol.* **2015,** *10*, 629-636.
6. Zhou, T.; Hong, G.; Fu, T.-M.; Yang, X.; Schuhmann, T. G.; Viveros, R. D.; Lieber, C. M. *Proc. Natl. Acad. Sci. U.S.A.* **2017,** *114*, 5894-5899.
7. Steif, P. S., *Mechanics of Materials*. Pearson: 2012.
8. Hong, G.; Fu, T.-M.; Zhou, T.; Schuhmann, T. G.; Huang, J.; Lieber, C. M. *Nano Lett.* **2015,** *15*, 6979-6984.
9. Quiroga, R. Q.; Reddy, L.; Kreiman, G.; Koch, C.; Fried, I. *Nature* **2005,** *435*, 1102.